 CMC, vol.18, no.2, pp.105-120, 2010

Theoretical Study on the Bilayer Buckling Technique for Thin Film Metrology

Fei Jia[1], Xiu-Peng Zheng[1,2], Yan-Ping Cao[1,3] and Xi-Qiao Feng[1]

Abstract: Recently, a novel technique based on the wrinkling of a bilayer composite film resting on a compliant substrate was proposed to measure the elastic moduli of thin films. In this paper, this technique is studied via theoretical analysis and finite element simulations. We find that under an applied compressive strain, the composite system may exhibit various buckling modes, depending upon the applied compressive strain, geometric and material parameters of the system. The physical mechanisms underlying the occurrence of the two most typical buckling modes are analyzed from the viewpoint of energy. When the intermediate layer is much thicker than the top layer, the condition under which the bilayer buckling will occur prior to other modes is given. The results reported here may facilitate the design of the bilayer buckling technique for the thin film metrology.

Keywords: Wrinkling, bilayer, thin film metrology, finite element method

1 Introduction

Thin film materials find wide applications as, for instance, sensors, actuators, functional coatings, optical reflectors and filters (Elshabini-Riad and Barlow, 1997; Freund and Suresh, 2003). Determining the mechanical properties of thin films is critical for the prediction of their performance in service. Several experimental methods have been proposed and widely applied in practice, e.g., micro-tension, bending, vibration, and nanoindentation tests (Nix, 1989; Hemker and Sharpe, 2007; Oliver and Pharr, 1992; Saha and Nix, 2002; Huber et al., 2002; Liu et al., 2008; Wu et al., 2009). Interpretation of the experimental data from micro-tension/bending and vibration tests is straightforward, but the preparation and handling of small-scale samples are rather difficult, especially when the film thickness reduces to nanometers. Nanoindentation tests are relatively easy to perform. However, correlating

[1] AML, Department of Engineering Mechanics, Tsinghua University, Beijing 100084, China
[2] CNNC China Nuclear Power Engineering Co., Ltd. Beijing 100840, China
[3] Corresponding author: Tel.: +86 10 62772520; e-mail: caoyanping@mail.tsinghua.edu.cn

the indentation responses with the mechanical properties is still a challenging issue since the measurement results may be influenced by many factors, e.g., the existence of indenter tip defects, complex interaction between the indenter and the sample (Qian et al., 2008), and substrate effects (Saha and Nix, 2002).

Recently, enlightened by the buckling phenomenon of thin films resting on a soft substrate (Bowden et al., 1998), Stafford et al. (2004) proposed a novel metrology, named "strain-induced elastic buckling instability for mechanical measurements" (SIEBIMM), to measure the elastic moduli of thin films. This method is based on the fundamental relation between the buckling wavelength and the geometric and material parameters of the system, and the elastic modulus of a thin film can be inversely calculated from the measured wavelength via the relation:

$$\frac{E_f}{1-\nu_f^2} = \frac{3E_s}{1-\nu_s^2}\left(\frac{\lambda_0}{2\pi h}\right)^3, \tag{1}$$

where E is the Young's modulus, ν the Poisson's ratio, λ_0 the wavelength, and h the thickness of the film. The subscripts " f " and " s " stand for the film and substrate, respectively.

Later on, the SIEBIMM method was extended to a wider range of problems, e.g., the mechanical characterization of films with finite width and micro/nano-wires or fibers (Nolte et al., 2006; Huang et al., 2007; Tarasovs and Andersons, 2008; Jiang et al., 2008; Zheng et al., 2009; Cao et al., 2009). The present paper investigates the bilayer buckling technique proposed by Nolte et al. (2006) for measuring the elastic moduli of thin films. By transferring a thin polystyrene film to an elastic poly-dimethylsiloxane (PDMS) surface prior to film deposition, Nolte et al. (2006) created a deposition surface that can promote the adhesion of films which are difficult to be directly transferred on PDMS. The thin bilayer composite films on a PDMS substrate may buckle like their homogeneous counterpart under compressions. Thus, the critical wrinkling wavelength of the bilayer can be estimated by that of a stiff layer resting on a soft substrate (Nolte et al., 2006), that is,

$$\lambda_{\mathrm{c}}^{\mathrm{bilayer}} = 2\pi h\left(\frac{E_{\mathrm{eff}}^*}{3E_s^*}\right)^{1/3}, \tag{2}$$

where $\lambda_{\mathrm{c}}^{\mathrm{bilayer}}$ is the wavelength and h the thickness of the bilayer composite film. $E^* = E/\left(1-\nu^2\right)$ is the plane-strain modulus, E and ν the Young's modulus and Poisson's ratio, respectively. The subscripts " s " and " eff " stand for the substrate and the bilayer composite film, respectively. The effective elastic modulus of the bilayer composite film in Fig. 1 can be written as (Nolte et al., 2006; Stafford et

al., 2005)

$$E_{\text{eff}}^{*} = \frac{1 + m^2 n^4 + 2mn\left(2n^2 + 3n + 2\right)}{(n+1)^3 (1+mn)} E_1^{*}, \tag{3}$$

where $m = E_2^{*}/E_1^{*}$, $n = h_2/h_1$, and h denotes a film thickness. The subscripts " 1 " and " 2 " stand for the surface layer and the intermediate layer, respectively. In the SIEBIMM method, E_{eff}^{*} can be measured from Eq. (3) and the known elastic properties of the substrate. Furthermore, for a given value of E_2^{*}, E_1^{*} can be determined and vice versa. Besides the merit as aforementioned, the bilayer bucking technique has the following advantages.

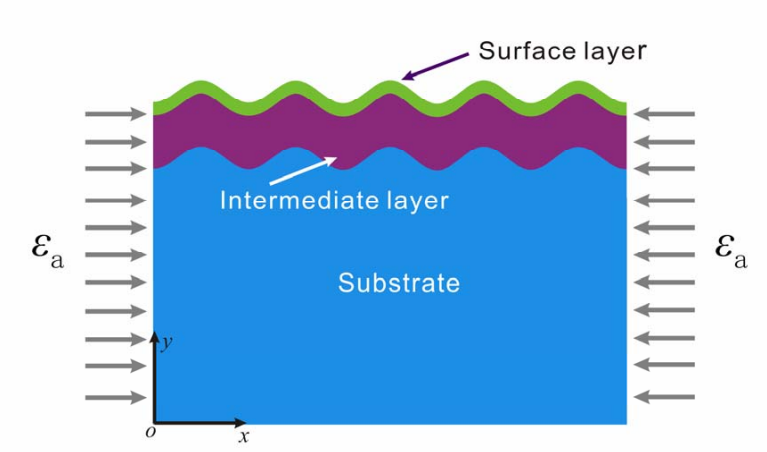

Figure 1: Schematic diagram of a bilayer buckling on a compliant substrate.

Firstly, when the intermediate layer is much thicker than the top one, the buckling wavelength of the bilayer will be much greater than that of a single thin film directly deposited on the substrate. Evidently, the magnified wrinkling wavelength is easier to be measured in practical experiments and renders a higher accuracy of measurement.

Secondly, the traditional SIEBIMM method has some constraints on the thin films. For example, when the elastic modulus of a thin film is not sufficiently large in comparison with that of the substrate, the film will be difficult to wrinkle. A promising treatment to overcome this difficulty is to first deposit a surface layer with a higher Young's modulus on the film to be measured, making the system easier to buckle .

In spite of these merits of the bilayer buckling technique, cautions should be taken to the buckling modes of the system in the practical design of experiments. As will be shown below, different buckling modes may occur in the composite system under study, depending on the applied compressive strain, geometric and material parameters. Therefore, it is necessary and important to identify the critical conditions under which the wrinkling of the bilayer occurs prior to other possible buckling modes. In this paper, we mainly consider the situation when the intermediate layer is much thicker than the surface layer. The corresponding buckling modes will be investigated by examining the total potential energy of the system. A phase diagram for the occurrence of the surface layer wrinkling, the bilayer buckling and the stable region will be provided with respect to the geometric and material parameters. Finite element simulations will be also performed to track the post-buckling behavior and to validate the theoretical solution.

2 Computational model

Consider a bilayer film lying on a compliant substrate, as shown in Fig. 1. The films and substrate are all assumed to be linearly elastic and isotropic. We mainly analyze the case where the intermediate layer is more compliant but much thicker than the surface layer. The substrate is infinite in thickness, and the system is treated as a plane-strain problem. Refer to a Cartesian coordinate system (*o-xy*), as shown in Fig.1, where the origin O is located at the left end of the bottom boundary of the substrate, and the x and y axes are along and normal to the surface layer, respectively. The left and right boundaries are specified with an increasing compressive displacement, the bottom surface is constrained in the y direction, and all the other boundaries are traction-free. The compressive strain ε_a is calculated by the compressive displacement divided by the total length of the film. When the compressive strain ε_a reaches a critical value, ε_c, wrinkling will occur on the surface of the system.

In the aforementioned bilayer buckling method suggested by Nolte et al. (2006), the elastic modulus of the thin film is inversely calculated from the measured buckling wavelength, by utilizing the fundamental relation in Eqs. (2) and (3). It is worth noticing that the application of this novel technique requires careful examinations of the buckling modes of the system. First, Eq. (2) gives the critical buckling wavelength corresponding to the critical compressive strain, $\varepsilon_c^{\text{bilayer}}$, at which the bilayer starts to wrinkle. In practice, however, the post-buckling wavelength is generally measured under a certain compressive strain ε_a, which should be larger than $\varepsilon_c^{\text{bilayer}}$. Therefore, of necessity is to quantitatively examine the validation scope of Eq. (2). Furthermore, it is emphasized that the simultaneous wrinkling of the two layers is only one of several possible buckling modes for the composite system in

Fig. 1. Besides this mode, the sinusoidal wrinkling or even hierarchical wrinkling of the surface layer may also happen, depending on the applied compressive strain, geometric and material parameters of the system. These buckling modes are not favorable for the application of the bilayer buckling measurement technique. Bearing these important issues in mind, we will perform finite element simulations to track the post-buckling behavior of the system under study.

Prior to the post-buckling analysis, a linear perturbation procedure is accomplished by using the BUCKLE function in the software. The most critical eigenmode scaled by a factor of 0.5% is introduced as a geometric imperfection into the mesh during our post buckling analysis. We have verified that such a small geometric perturbation basically has no effect on the post-buckling behavior. For post-buckling analysis, the well-established arc-length method initiated by Riks (1979) and improved by some other researchers (Powell and Simons, 1981; Ramm, 1981; Crisfield, 1981, 1983) has been widely and successfully adopted for many global buckling problems. However, this method is difficult to treat problems with equilibrium branches. In such situations, the stabilized Newton-Raphson method is generally recommended (Tafreshi, 2004; ABAQUS, 2008). Therefore, we here use the stabilized Newton-Raphson method, instead of the arc-length method. This algorithm can easily solve unstable problems through the automatic addition of volume-proportional damping to the model. The viscous forces of the structure is given by

$$F_{\mathrm{v}} = cMv, \tag{4}$$

where M is an artificial mass matrix calculated with unity density, c is a damping factor, $v = \Delta u/\Delta t$ is the vector of nodal velocities, and Δt is the increment of time.

This algorithm adopts an adaptive automatic stabilization scheme (ABAQUS, 2008), in which the damping factor can vary spatially and temporally and is controlled by the convergence history. When the convergence behavior is problematic due to instabilities, the algorithm will automatically increase the damping factor. On the other hand, the damping factor will be automatically reduced if instability subsides. This technique has been successfully used to analyze the buckling of a film with finite width or a fiber resting on a compliant substrate (Zheng et al., 2009; Cao et al., 2009).

The interfaces between the surface layer, the intermediate layer and the substrate are perfectly bonded by using 'tie' constraints in commercial software ABAQUS (Version 6.8). This study focuses on the case where the film is perfectly bonded to a soft substrate. First, many recent experiments (e.g. Bowden et al., 1998; Stafford et al. 2004; Nolte et al., 2006) have shown that the assumption of perfect bonding can be easily realized in practice. Second, our recent computational studies

(Zheng et al., 2009; Cao et al., 2009) indicate that for a film with finite width or a fiber resting on a soft substrate, the assumption of a uniform normal stress distribution along the contact width is acceptable for predicting the buckling wavelength. This finding implies that when small scale debonding occurs, the local strains and stresses at the debonding places may change but the global buckling wavelength will not vary. Finally, it is pointed out that when large scale delamination happens, the analysis and corresponding conclusions should be modified. Eight-node plane-strain quadrilateral reduced integration elements (CPE8R) are used both for the films and substrate. Fig. 2 represents the mesh of the computational model used in the simulations.

Convergence analysis is carried out for each case. The effects of the substrate dimensions are carefully examined, which are chosen to be sufficiently large such that the solutions are insensitive either to the substrate sizes or the external boundary conditions.

3 Results and discussions

3.1 Buckling modes of a bilayer composite film on a compliant substrate

Our computational results demonstrate that different buckling modes may occur in the system of current interest. The two most typical modes are the wrinkling of the single top layer, and the buckling of the two thin films as a whole, which will be referred to as mode-I and mode-II in the sequel, as shown in Fig. 2a and 2c, respectively. In addition, a hierarchical buckling (Fig. 2b, mode-III) following the occurrence of mode-I or mode-II is also observable with further increasing compressive strain. In the bilayer buckling technique, the mode-II buckling is adopted to measure the elastic modulus of a thin film, while modes-I and III should generally be avoided. Therefore, this requires a careful design of the experiment. For this purpose, the critical conditions for the occurrence of these buckling modes should be given, in conjunction with the fundamental relation between the buckling modes and the geometric and material parameters. Since the mode-III buckling can only be observed following the occurrence of mode-I or mode-II, our attention will be focused on the mode-I and mode-II in this study. The two buckling modes of the system correspond to two distinct mechanics models. The former can be considered as a monolayer wrinkling on a composite substrate, while the latter is a bilayer buckling on a homogeneous substrate. The physical mechanisms underling the occurrence of the buckling modes may be explained by examining the total potential energy of the system, as will be described below.

For the mode-I buckling, the wrinkling profile of the surface layer shown in Fig. 2

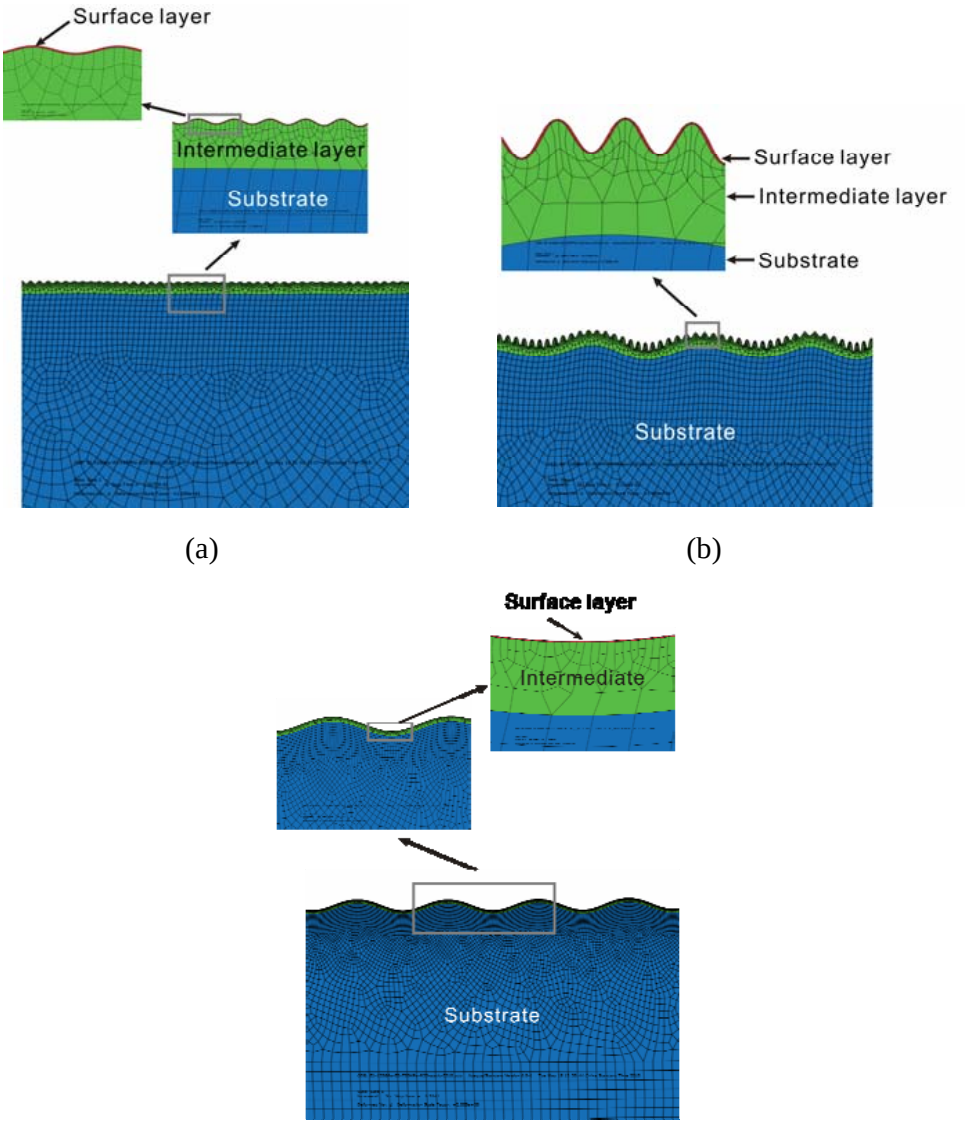

Figure 2: Simulation results of (a) surface layer buckling (mode-I), (b) hierarchical wrinkling (mode-III), and (c) bilayer buckling (mode-II). Finite element meshes used in the computations are also given.

may be expressed as

$$w^{\text{surface}} = w_0^{\text{surface}} \cos\left(k^{\text{surface}} x\right), \tag{5}$$

where w^{surface} is the deflection of the surface layer in the y-direction, w_0^{surface} and k^{surface} are the buckling amplitude and wavenumber, respectively. For such a buckling profile, the total potential energy of the system, $\Pi_{\text{tot}}^{\text{surface}}$, consists of the following four parts (Huang et al., 2005)

$$\Pi_{\text{tot}}^{\text{surface}} = U_{\text{m}}^{\text{surface}} + U_{\text{b}}^{\text{surface}} + U_{\text{s}}^{\text{surface}} + U_{\text{p}}^{\text{surface}}, \tag{6}$$

where $U_{\text{m}}^{\text{surface}}$ and $U_{\text{b}}^{\text{surface}}$ denote the membrane energy and the bending energy of surface layer, respectively, $U_{\text{s}}^{\text{surface}}$ is the elastic strain energy of the substrate, and $U_{\text{p}}^{\text{surface}}$ is the potential energy of the externally applied loads.

According to the principle of minimal potential energy, the elasticity of the substrate is inclined to generate smaller wavelengths, whereas the bending of the top layer favors larger wavelengths. Therefore, there exists an optimum wavenumber $k_{\text{optimal}}^{\text{surface}}$ that minimizes the total potential energy, denoted as $\Pi_{\text{tot - buckle}}^{\text{surface}}$ (Groenewold, 2001). Under a small compressive strain and before the occurrence of surface buckling, the composite system bears a uniform compressive deformation and the total potential energy is symbolized as $\Pi_{\text{tot - comp}}$. Obviously, the wrinkling of surface layer occurs only when the condition of $\Pi_{\text{tot - comp}} = \Pi_{\text{tot - buckle}}^{\text{surface}}$ is satisfied.

For the mode-II or bilayer buckling, the wrinkling profile of the bilayer may assume

$$w^{\text{bilayer}} = w_0^{\text{bilayer}} \cos\left(k^{\text{bilayer}} x\right), \tag{7}$$

where w^{bilayer} is the deflection of the bilayer in the y direction, w_0^{bilayer} and k^{bilayer} denote the buckling amplitude and wavenumber, respectively. Similarly, there exists an optimum wavenumber $k_{\text{optimal}}^{\text{bilayer}}$ which minimizes the total potential energy of the system. Let $\Pi_{\text{tot - buckle}}^{\text{bilayer}}$ denote total potential energy corresponding to the optimum wavenumber $k_{\text{optimal}}^{\text{bilayer}}$. Hence, the occurrence of the bilayer buckling requires

$$\Pi_{\text{tot - comp}} = \Pi_{\text{tot - buckle}}^{\text{bilayer}}. \tag{8}$$

The above analysis shows that the system selects a specific buckling mode according to the following condition

$$\Pi_{\text{tot - comp}} = \min\left(\Pi_{\text{tot - buckle}}^{\text{bilayer}}, \Pi_{\text{tot - buckle}}^{\text{surface}}\right). \tag{9}$$

The bilayer buckling technique assumes that mode-II occurs prior to mode-I. In other words, the condition of $\Pi^{\text{bilayer}}_{\text{tot - buckle}} < \Pi^{\text{surface}}_{\text{tot - buckle}}$ should be met in the design of experiments. Furthermore, since the hierarchical wrinkling shown in Fig. 2b can only appear after the occurrence of mode-I buckling, it will have a higher total potential energy of the system. Therefore, the condition of $\Pi^{\text{bilayer}}_{\text{tot - buckle}} < \Pi^{\text{surface}}_{\text{tot - buckle}}$ can ensure that neither mode-I nor mode-III buckling can happen before mode-II. However, such a condition based on the energy argument is not very convenient for practical applications because of the difficulty in the calculation of the total potential energy. In the next section, therefore, we will provide a critical condition in terms of the compression strain.

3.2 Critical condition for bilayer wrinkling as a whole

When the applied strain ε_{a} is small, the system is stable and undergoes uniform compressive deformation. With the increase in the compressive strain, either the surface layer or the bilayer will wrinkle. In this study, we are particularly interested in the case where the intermediate layer is much thicker than the top (e.g., the thickness ratio is larger than 50 times) such that the wavelength can be easily measured. Under this circumstance, the influence of the substrate may be negligible. When the surface layer wrinkles first, the critical strain corresponding to $\Pi_{\text{tot - comp}} = \Pi^{\text{surface}}_{\text{tot - buckle}}$ reads (Huang et al., 2005)

$$\varepsilon_{\text{c}}^{\text{surface}} = \frac{1}{4}\left(\frac{3E_2^*}{E_1^*}\right)^{\frac{2}{3}}. \tag{10}$$

For the case where the bonded surface and intermediate layers (bilayer) buckle as a whole, just like their homogeneous counterpart on the substrate, the critical compressive strain corresponding to $\Pi_{\text{tot - comp}} = \Pi^{\text{bilayer}}_{\text{tot - buckle}}$ gives

$$\varepsilon_{\text{c}}^{\text{bilayer}} = \frac{1}{4}\frac{E^*_{\text{eff}}}{E^*_{\text{t}}}\left(\frac{3E^*_{\text{s}}}{E^*_{\text{eff}}}\right)^{\frac{2}{3}}, \tag{11}$$

where E^*_{s} is the plane-strain moduli of the substrate and E^*_{eff} is the effective modulus of the bilayer composite film in tension (Huang et al., 2007).

The critical condition under which the mode-II buckling happens before mode-I can be derived from Eqs. (10) and (11). Simply, the condition $\varepsilon_{\text{c}}^{\text{surface}} > \varepsilon_{\text{c}}^{\text{bilayer}}$ provides a guideline for the practical design of experiments. Under a representative parameter combination of h_2/h_1, E_1^* and E_s^*, Fig. 3 gives a phase diagram for the occurrence of the surface layer wrinkling, the bilayer buckling and the stable region. The composite system is stable and experiences uniform compressive

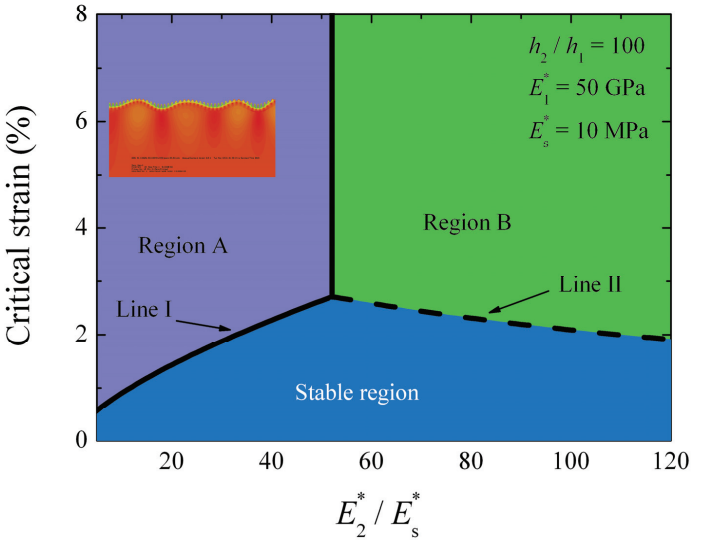

Figure 3: A phase diagram for the occurrence of surface layer wrinkling (Line I), bilayer buckling (Line II), and the stable region, where E_1=50 GPa, E_s=10 MPa, and h_2/h_1=100. In both Region A and B, when the compressive strain is large enough, hierarchical wrinkling may occur as illustrated in Region A.

deformation when the applied compressive strain ε_a is smaller than the critical values on the curves I and II. The mode-I buckling will occur first when the strain ε_a reaches the curve I, i.e., the lower boundary of Region A. With increasing ε_a, the hierarchical wrinkling may occur in Region A, as shown in the inset of Fig. 3. Region B defines the scope of the applied strain in which the mode-II buckling appears prior to mode-I. In other words, when the strain ε_a reaches the critical values of the curve II, the bilayer wrinkling will be preferable. However, it is also mentioned that in this region, the hierarchical wrinkling can also occur when the compressive strain is too large. Therefore, cautions should be taken to this point in practical measurements.

Fig. 4 illustrates the critical condition with respect to different ratios of E_2^*/E_s^*. It is seen that for given values of h_2/h_1, E_1^* and E_s^*, the ratio of E_2^*/E_s^* should be larger than a certain critical value (circle points) in order to guarantee the prior occurrence of the mode-II buckling. Fig. 4 also shows that the ratio h_2/h_1 should be smaller than the critical values so that the bilayer buckling technique can be steadily applied. In the design of such an experiment, one should first estimate the ratio h_2/h_1 by using the prior knowledge of E_1^*, E_s^* and E_2^*.

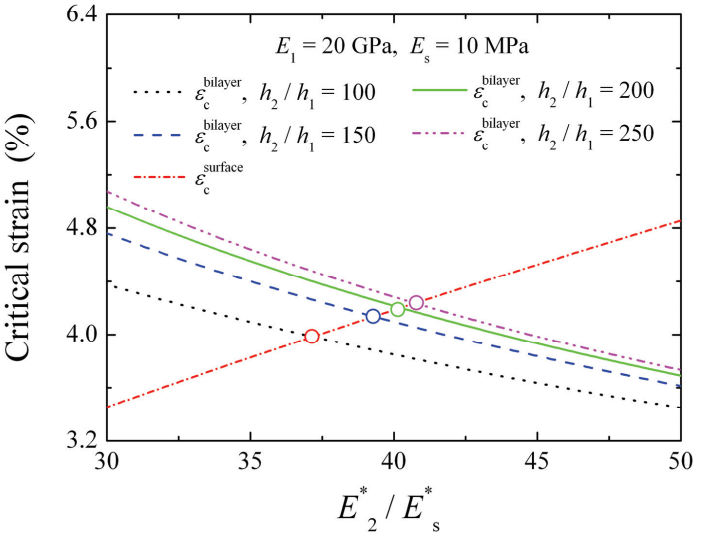

Figure 4: Variations of the critical strains $\varepsilon_c^{surface}$ and $\varepsilon_c^{bilayer}$ with respect to the normalized modulus of the intermediate layer E_2^*/E_s^* for several thickness ratios of h_2/h_1, where we take E_1=20 GPa, E_s=10 MPa. The circles indicate the critical points beyond which the buckling of bilayer occurs first.

In order to quantitatively examine the applicability of Eq. (2) to the post-buckling process and also validate the critical condition as presented above, a series of finite element simulations are performed. The Young's modulus and Poisson's ratio of the substrate are taken as E_s=10 MPa and ν_s=0.45, respectively. The Poisson's ratios of the surface and intermediate layers are ν_1=0.3 and ν_2=0.45, respectively. Two combinations of (E_1, h_2/h_1), i.e., (E_1=50 GPa, h_2/h_1=100) and (E_1=120 GPa, h_2/h_1=50) are investigated. For these two cases, the critical value of E_2 of the intermediate layer beyond which the mode-II buckling appears prior to mode-I are determined, from Eqs. (10) and (11), as 521 MPa and 298 MPa, respectively. In order to validate the critical condition suggested above by theoretical analysis, we compare the simulation results for various values of E_2 in a wide range. The wrinkling wavelengths extracted from finite element simulations are shown in Fig. 5. The solid line in Fig. 5a is the theoretical results derived from Eq. (2) for the surface layer buckling, where E_{eff}^* and E_s^* have been replaced by E_1^* and E_2^*, while the solid line in Fig. 5b is calculated by Eqs. (2) and (3). Clearly, the finite element results agree well with the theoretical predictions, with the relative errors below 4.0%. Fig. 5 demonstrates that indeed the mode-I buckling appears first when E_2 is

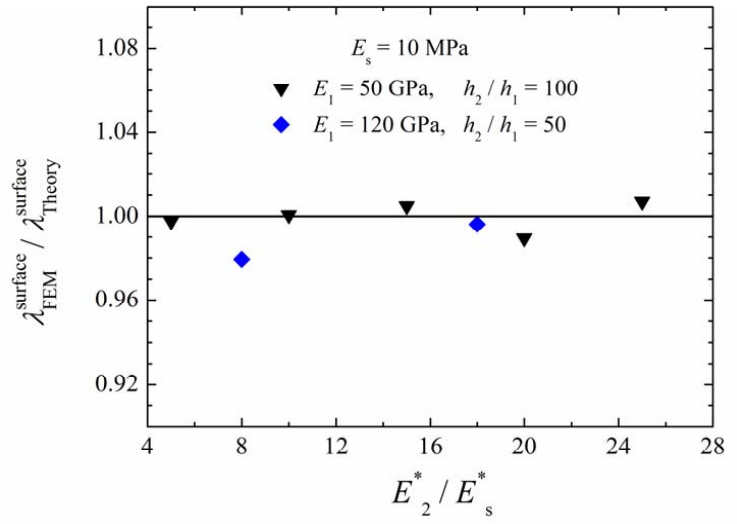

(a)

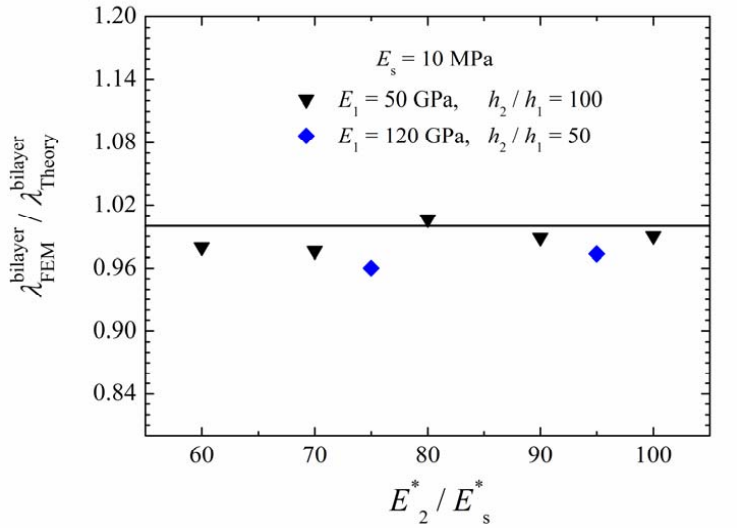

(b)

Figure 5: Relative differences of the wrinkling wavelength obtained from finite element simulation ($\lambda_{FEM}^{surface}$ or $\lambda_{FEM}^{bilayer}$) and the corresponding theoretical analysis ($\lambda_{Theory}^{surface}$ or$\lambda_{Theory}^{bilayer}$). (a) $\lambda_{FEM}^{surface}$ and $\lambda_{Theory}^{surface}$, and (b) $\lambda_{FEM}^{bilayer}$ and $\lambda_{Theory}^{bilayer}$.

smaller than the critical value determined by our theoretical analysis, and the mode-II buckling will occur for a larger E_2. Therefore, the critical condition established from Eqs. (10) and (11) provides a guideline for experimental design.

Fig. 5 shows that the wavelengths obtained from finite element simulations are slightly smaller than the theoretical prediction given by Eqs. (2) and (3). This is because finite element simulations give post-buckling wavelength, while the solution derived by Eqs. (2) and (3) corresponds to the critical buckling condition. According to the inextensibility condition of the film, the measured wavelength will decrease with the increase in the applied strain. According to a very recent analysis (Brau et al., 2010), the evolution of the wavelength λ along the horizontal direction can be simply given by

$$\frac{\lambda}{\lambda_c} = 1 - \varepsilon_a. \tag{12}$$

Therefore, in order to use the analytical solution as a fundamental relation of the bilayer buckling technique to measure the elastic modulus of a thin film, either the applied strain should be very small, i.e., $\varepsilon_a << 1$, or the solutions should be modified by including the effects of ε_a (Jiang et al., 2007; Brau et al., 2010).

4 Conclusions

The wrinkling phenomenon of a bilayer composite film resting on a compliant substrate under in-plane compression finds applications in thin film metrology. In this study, we show that such a composite system may exhibit various post-buckling modes, depending on the applied compressive strain, material and geometric parameters of the system, which should be considered in the bilayer buckling technique. We elucidate the physical mechanisms for the occurrence of a specific buckling mode. The condition under which the system will first undergo a bilayer buckling is given. These results may help the design of experiments when the bilayer buckling technique is used for the mechanical characterization of thin films.

Acknowledgement: Supports from the National Natural Science Foundation of China (Grant Nos. 10972112, and 10732050) and 973 Program (2010CB631005) are acknowledged.

References

ABAQUS (2008): ABAQUS analysis user's manual, version 6.8.

Bowden, N.; Brittain, S.; Evans, A. G.; Hutchinson, J. W.; Whitesides, G. M. (1998): Spontaneous formation of ordered structures in thin films of metals

supported on an elastomeric polymer. *Nature*, vol. 393, pp. 146-149.

Brau, F.; Vandeparre, H.; Sabbah, A.; Poulard, C.; Boudaoud, A.; Damman, P. Multiple-length-scale elastic instability mimics parametric resonance of nonlinear oscillators. Nature Phys. (in press).

Cao, Y. P.; Zheng, X. P.; Li, B.; Feng, X. Q. (2009): Determination of the elastic modulus of micro- and nanowires/tubes using a buckling-based metrology. *Scripta Mater*, vol. 61, pp. 1044-1047.

Crisfield, M. A. (1981): A fast incremental-iterative solution procedure that handles snap-through. *Comput Struct*, vol. 13, pp. 55-62.

Crisfield, M. A. (1983): An arc-length method including line searches and accelerations. *Int J Numer Meth Eng*, vol. 19, pp. 1269-1289.

Elshabini-Riad, A. A. R.; Barlow, F. D. (1997): Thin Film Technology Handbook, McGraw-Hill, Newyork.

Freund, L. B.; Suresh, S. (2003): Thin Film Materials, Cambridge University Press, Cambridge, UK.

Groenewold, J. (2001): Wrinkling of plates coupled with soft elastic media. *Phys A*, vol. 298, pp. 32-45.

Hemker, K. J.; Sharpe, W. N. (2007): Microscale characterization of mechanical properties. *Annu Rev Mater Res*, vol. 37, pp. 93-126.

Huang, R.; Stafford, C. M.; Vogt, B. D. (2007): Effect of surface properties on wrinkling of ultrathin films. *J Aerospace Eng*, vol. 20, pp. 38-44.

Huang, Z. Y.;Hong, W.; Suo, Z. (2005): Nonlinear analyses of wrinkles in a film bonded to a compliant substrate. *J Mech Phys Solids*, vol. 53, pp. 2101-2118.

Huber, N.; Nix, W. D.; Gao, H. (2002): Indentation of elastic-plastic material parameters from pyramidal indentation of thin films. *Proc R Soc Lond A*, vol. 458, pp. 1593-1620.

Jiang, H. Q.; Khang, D. Y.; Song, J. Z.; Sun, Y. G.; Huang, Y. G.; Rogers, J. A.; (2007): Finite deformation mechanics in buckled thin films on compliant supports. *Proc. Natl. Acad. Sci. USA*, vol. 104, pp. 15607

Jiang, H. Q.; Khang, D. Y.; Fei, H. Y.; Kim, H.; Huang, Y. G.; Xiao, J. L.; Rogers, J. A. (2008): Finite width effect of thin-films buckling on compliant substrate: Experimental and theoretical studies. *J Mech Phys Solids*, vol. 56, pp. 2585-2598.

Liu, C. S.; Chang, J. R.; Chang, K. H.; Chen, Y. W. (2008): Simultaneously estimating the time-dependent damping and stiffness coefficients with the aid of vibrational data. *Comput Mater Con*, vol. 7, pp. 97-107.

Nix, W. D. (1989): Mechanical-properties of thin-films. *Metal Trans A*, vol. 20, pp. 2217-2245.

Nolte, A. J.; Cohen, R. E.; Rubner, M. F. (2006): A two-plate buckling technique for thin film modulus measurements: applications to polyelectrolyte multilayers. *Macromolecules*, vol. 39, pp. 4841-4847.

Oliver, W. C.; Pharr, G. M. (1992): An improved technique for determining hardness and elastic modulus using load and displacement sensing indentation experiments. *J Mater Res,* vol. 7, pp. 1564-1583.

Powell, G.; Simons, J. (1981): Improved iteration strategy for nonlinear structures. *Int J Numer Meth Eng*, vol. 17, pp. 1455-1467.

Qian, X.; Cao, Y.; Zhang, J.; Raabe, D.; Yao, Z.; Fei, B. (2008): An inverse approach to determine the mechanical properties of elastoplastic materials using indentation tests. *Comput Mater Con*, vol. 7, pp. 33-41.

Ramm, E. (1981). Strategies for tracing the nonlinear response near limit points. In: E. Stein and K. J. Bathe (ed) *Nonlinear Finite Element Analysis in Structural Mechanics*. Springer-Verlag, New York, 63-89.

Riks, E. (1979): Incremental approach to the solution of snapping and buckling problems. *Int J Solids Struct*, vol. 15, pp. 529-551.

Saha, R.; Nix, W. D. (2002): Effects of the substrate on the determination of thin film mechanical properties by nanoindentation. *Acta Materialia*, vol. 50, pp. 23-38.

Stafford, C. M.; Guo, S.; Harrison, C.; Chiang, M. Y. (2005): Combinatorial and high-throughput measurements of the modulus of thin polymer films. *Rev Sci Instrum*, vol. 76, pp. 062207.

Stafford, C. M.; Harrison, C.; Beers, K. L.; Karim, A.; Amis, E. J.; Vanlandingham, M. R.; Kim, Ho-C.; Volksen, W.; Miller, R. D.; Simonyi, E. E. (2004): A buckling-based metrology for measuring the elastic moduli of polymeric thin films. *Nat Mater*, vol. 3, pp. 545-550.

Tafreshi, A. (2004): Delamination buckling and postbuckling in composite cylindrical shells under external pressure. *Thin Wall Struct*, vol. 42, pp. 1379-1404.

Tarasovs, S.; Andersons, J. (2008): Buckling of a coating strip of finite width bonded to elastic half-space. *Int J Solids Struct*, vol. 45, pp. 593-600.

Wu, C. J.; Chou, C. Y.; Han, C. N.; Chiang, K. N. (2009): Estimation and validation of elastic modulus of carbon nanotubes using nano-scale tensile and vibrational analysis. *Comp Model Eng*, vol. 41, pp. 49-67.

Zheng, X. P.; Cao, Y. P.; Li, B.; Feng, X. Q.; Jiang, H. Q.; Huang, Y. G. (2009): Determining the elastic modulus of thin films using a buckling-based method: com-

putational study. *J Phys D Appl Phys*, vol. 42, pp. 175506.